Electronic Supplementary Material (ESI) for RSC Advances.
This journal is © The Royal Society of Chemistry 2023

Supplementary material for

Robust Method for Uniform Coating of Carbon Nanotubes with V_2O_5 for Next-Generation Transparent Electrodes and Li-ion Batteries

Daniil A. Ilatovskii,[a] Dmitry V. Krasnikov,[a] Anastasia E. Goldt,[a] Seyedabolfazl Mousavihashemi,[b] Jani Sainio,[b] Eldar M. Khabushev,[a] Alena A. Alekseeva,[a] Sergey Yu. Luchkin,[a] Zakhar S. Vinokurov,[c] Alexander N. Shmakov,[c] Aly Elakshar,[a] Tanja Kallio*[b], and Albert G. Nasibulin[a]*

[a] *Skolkovo Institute of Science and Technology, Bolshoy Boulevard 30, bd. 1, Moscow, 121205, Russian Federation.*

[b] *Aalto University, Kemistintie 1, 02150 Espoo, Finland.*

[c] *Boreskov Institute of Catalysis SB RAS, Lavrentieva avenue 5, Novosibirsk, 630090, Russian Federation*

* *e-mails: tanja.kallio@aalto.fi, a.nasibulin@skol.tech*

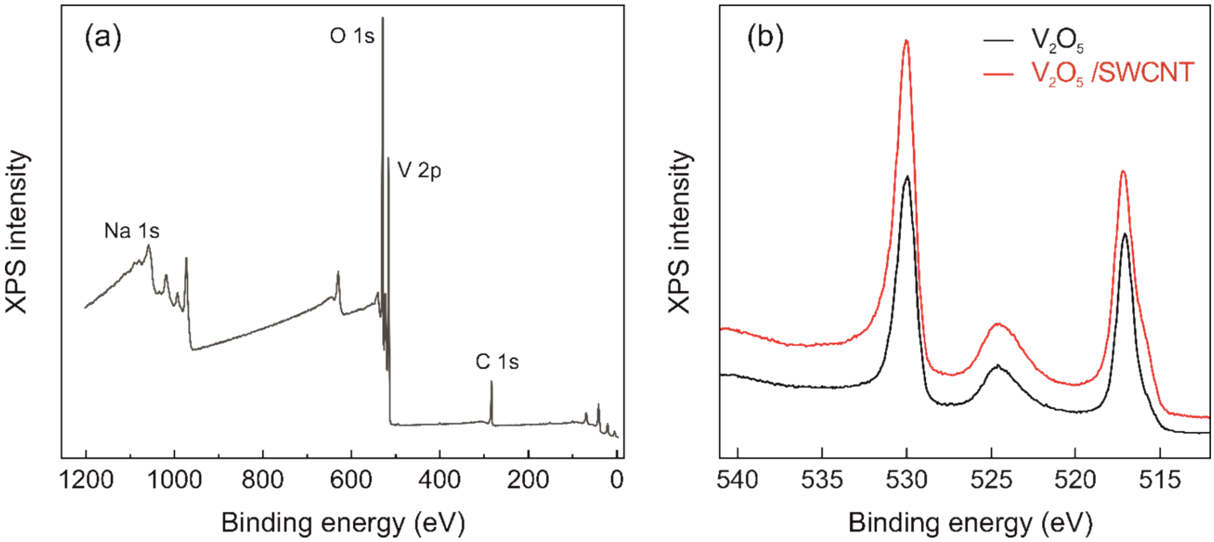

Figure S1. XPS survey spectrum of the V_2O_5/SWCNT composite (a), trace amount of Na (with an atomic concentration about 1%) was found here as an impurity; O 1s−V 2p region of the bare V_2O_5 and V_2O_5/SWCNT composite material (b).

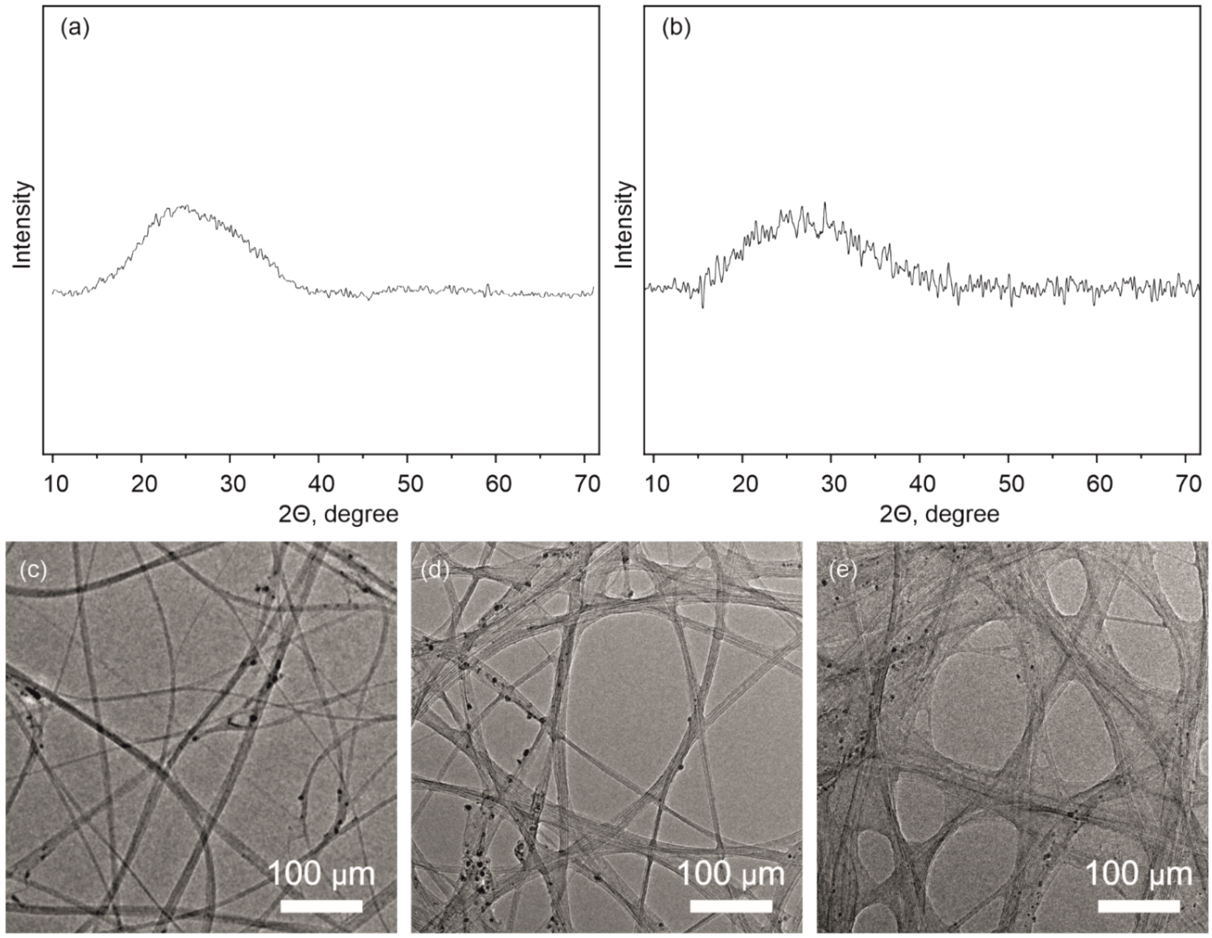

Figure S2. XRD pattern of the pristine SWCNT film (a) and V_2O_5/SWCNT composite (b), TEM images of SWCNTs doped by 0 (c), 9 (,d) and 42 (e) µM solution of VTIP. TEM images reveal iron nanoparticles –active and inactive catalyst formed due to the decomposition of ferrocene.

Table S1. Sheet resistance values for samples from **Fig. 3**.

The number of days after coating	R_s, Ω/sq					
	9µM VTIP Synthesis in Air Storage in Air at 25°C, 40% RH	18µM VTIP Synthesis in Air Storage in Air at 25°C, 40% RH	9µM VTIP Synthesis in Air Storage in N_2 at 25°C, 40% RH	9µM VTIP Synthesis in Air Storage in Air at 35°C, 100% RH	9µM VTIP Synthesis in Air Storage in Air at 60°C, 100% RH	9µM VTIP Synthesis in N_2 Storage in N_2 at 25°C, 0% RH
0 ($R_s = R_0$)	125	153	128	131	126	129
1	130	162	135	171	162	133
2	133	173	138	171	163	142

SWCNTs.

3	135	175	141	171	162	148
4	136	178	144	171	162	154
5	137	180	147	171	162	158
6	138	189	150	170	162	167
8	140	190	154	171	162	175
10	144	193	156	171	162	221
12	150	195	160	171	162	-
14	154	196	161	171	162	-
16	158	200	164	171	162	-
18	159	200	166	172	162	-
20	160	201	167	171	161	-
25	162	201	168	171	162	-
30	161	200	168	172	162	-
35	162	201	169	171	162	-
50	160	201	169	171	162	-

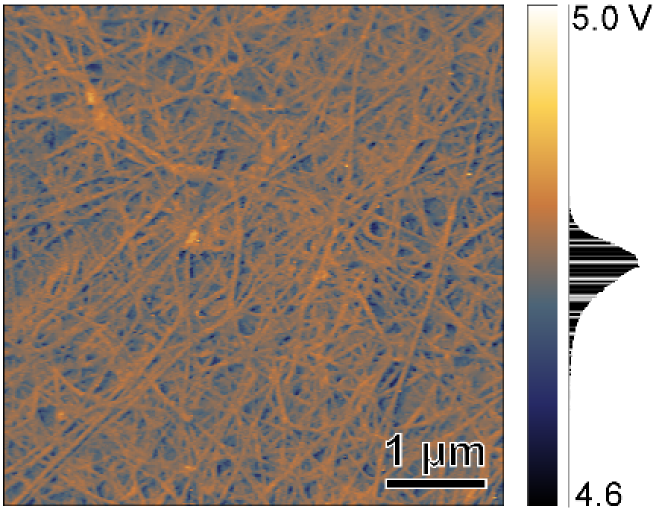

Figure S3. Results of Kelvin Probe Force Microscopy showing work function for the pristine SWCNTs.

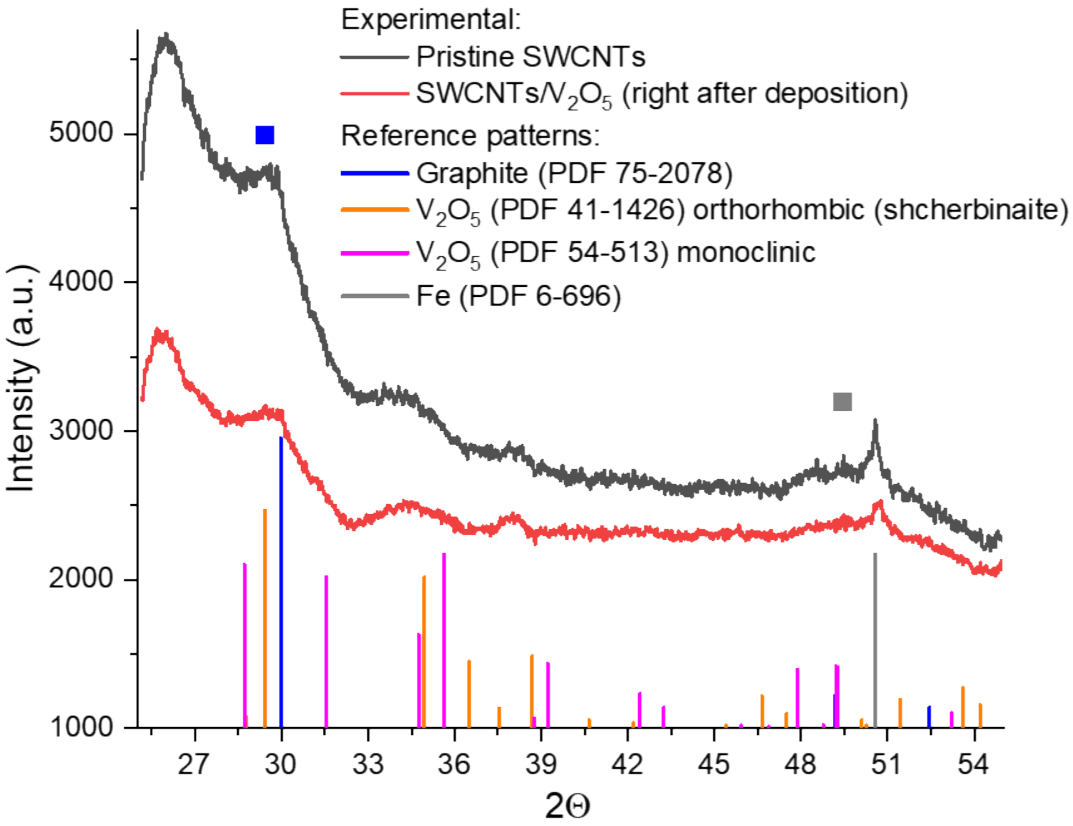

Figure S4. Typical in situ XRD patterns of pristine SWCNTs (black) and the same SWCNTs covered with V_2O_5 (red); database PDF patterns of graphite (blue), V_2O_5 (orthorhombic (orange), and monoclinic (magenta)), and iron (grey).

As the penetration depth of X-ray diffraction spans beyond microns as well as due to the architecture of the holder for the in situ XRD reactor chamber, we shifted from the SWCNT films toward the nanotube powder. Single-walled carbon nanotubes were purchased from OCSiAl company (Novosibirsk, Russia). To avoid any influence of catalyst residuals, the powder was subjected to heating (air, 400°C, 2 h) followed by HCl reflux treatment (8 h). Curiously, we still observe a small fraction of catalyst (presumably encapsulated within the nanotube channels) as well as C(002) reflex corresponding to multilayer graphitic structure (i.e. multi-walled carbon nanotubes in our case) in XRD spectra (Figure S4). The presence of MWCNTs was confirmed with TEM studies (not shown here). The peak Fe corresponds to iron based catalyst nanoparticles.

The addition of VTIP/IPA solution on the same SWCNT powder (already in the XRD holder) as well as forthcoming drying at room temperature does not result in any changes in the XRD pattern. Considering the extreme brightness of synchrotron radiation XRD as well as the small instrumental broadening of the reflexes, which allows us to detect crystallites up to 5-7 nm, we can state that the V_2O_5 formed is amorphous.

Heating of V_2O_5/SWCNT was performed in the mixture of pure He and O_2 (referred to as "air" hereafter). Using FMC Sierra mass-flow controllers, we maintained the oxygen concentration in helium at 21 vol. %. Crystallization appears only after *ca.* 450 ^{o}C (Figure S5 a). Interestingly, this process coincides with nanotube burning observed by both XRD (Figure S5 a) and mass-spectroscopy (Figure S5 b). The nanotube burning also changes the volume of the sample (Figure S5 c) breaking the precision of the reflex assignment. Moreover, heating itself affects the lattice parameters due to the positive thermal expansion coefficient. Thus, we can rather qualitatively assign phases for the heated pattern (Figure S5 c). Most likely, we observe a mixture of monoclinic (PDF # 54-513) and orthorhombic (PDF # 41-1426) V_2O_5 phases.

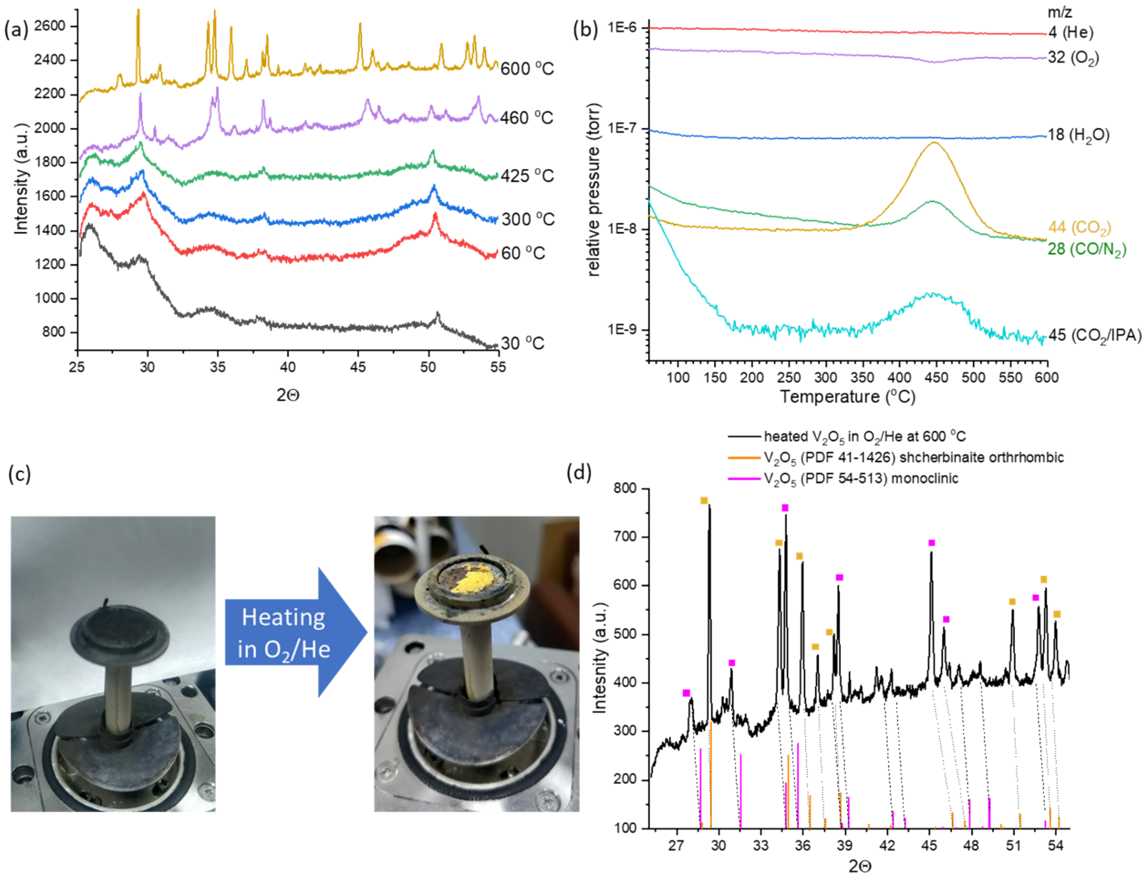

Figure S5. In situ XRD patterns of V_2O_5/SWCNT during heating in "air" (a); temperature dependence of designated m/z signals of the mass spectrometer with the proposed gas species; photos of the XRD holder before and after heating in the air; in situ XRD pattern of the sample heated at 600 ^{o}C in "air"(d).

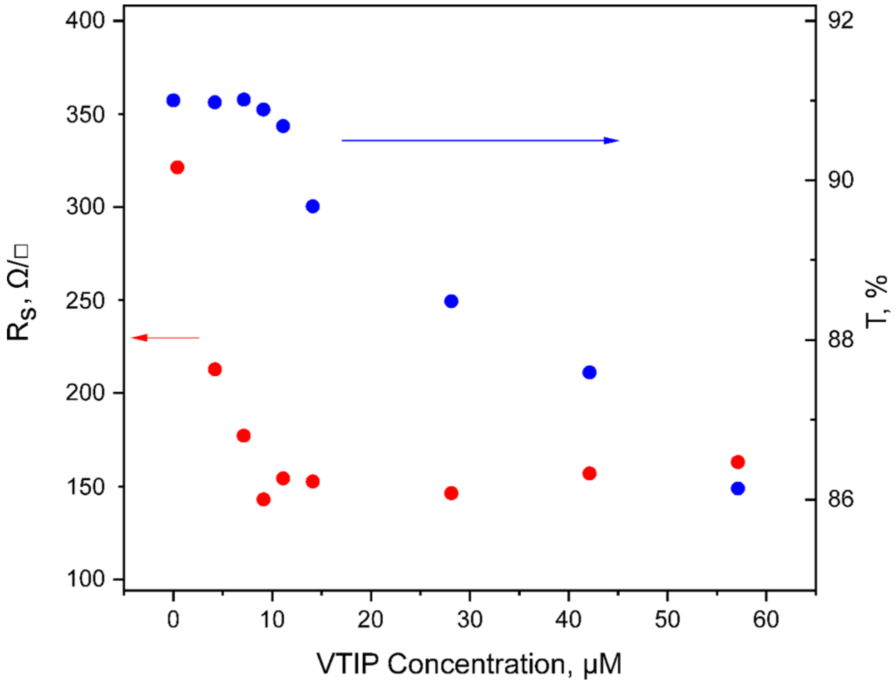

Figure S6. The concentration of dopant precursor *vs* sheet resistance (R_s) – red dots and transmittance (T) – blue dots of doped SWCNTs (left) for 1 cm^2 film.

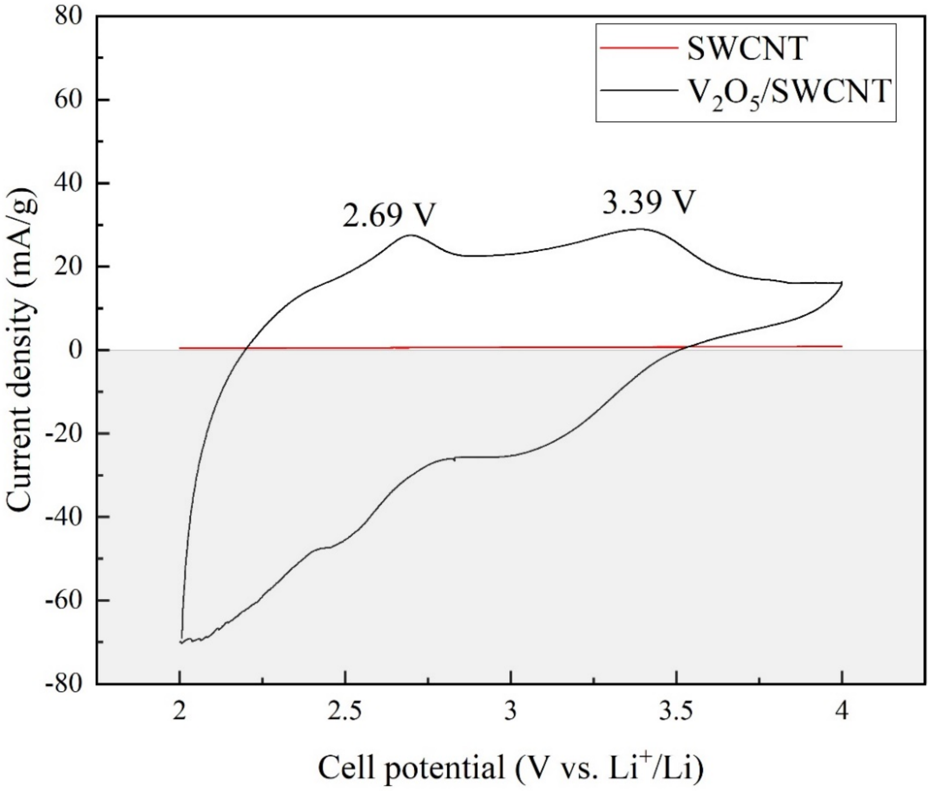

Figure S7. Cyclic voltammetry of SWCNT and V_2O_5/SWCNT at 0.02 mV/s scan rate in a three-electrode assembly.

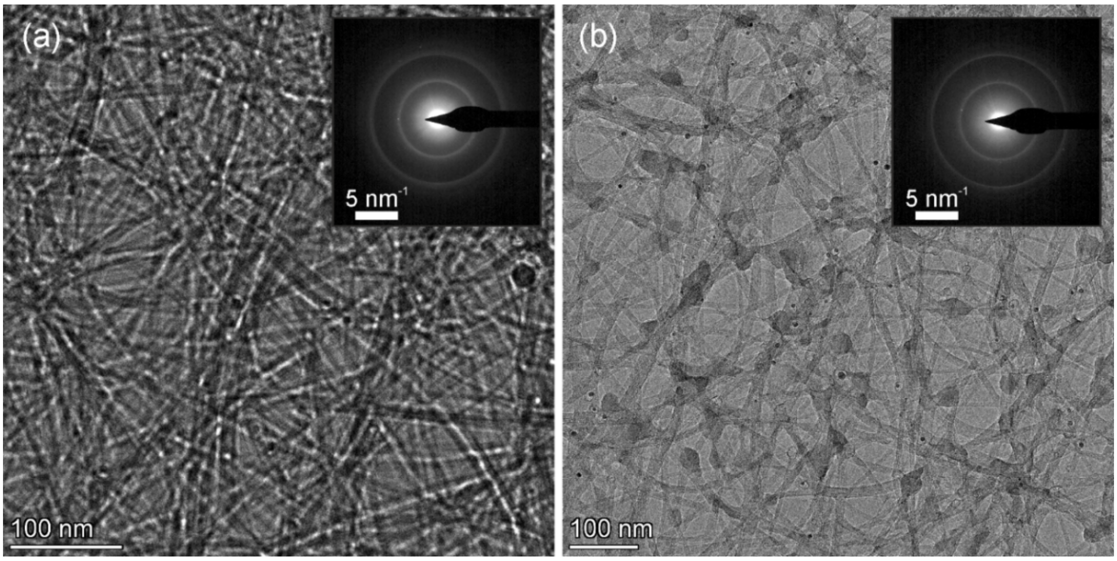

Figure S8. Selected area diffraction pattern and TEM image of pristine SWCNT film (a) and V_2O_5/SWCNT composite (b). The absence of extra rings in the diffraction pattern of the composite compared to pristine film demonstrates that the V_2O_5 coating is not microcrystalline.

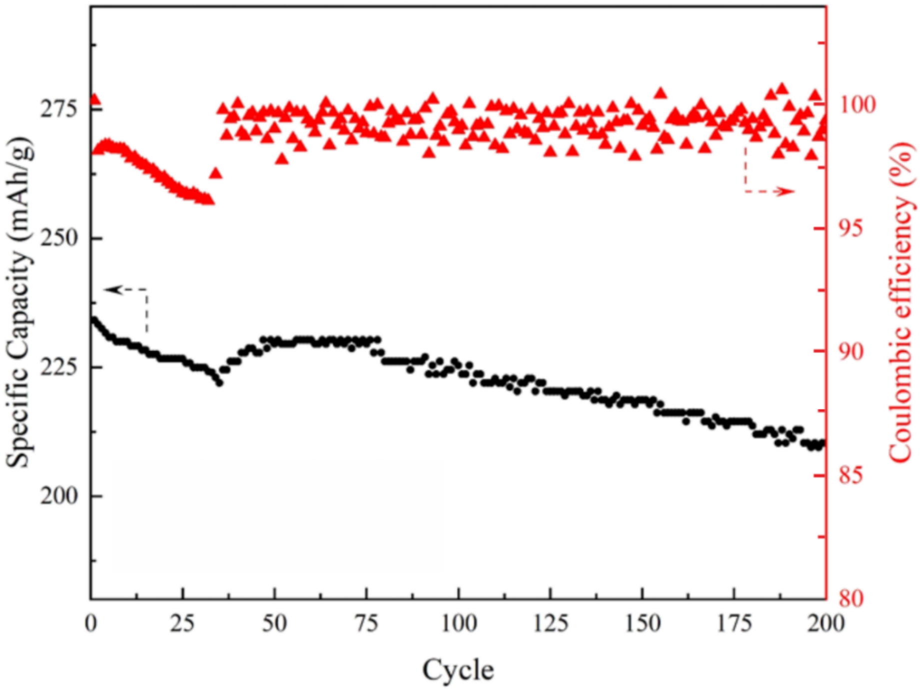

Figure S9. Cycling performance of V_2O_5/SWCNT at 1*C* (between 2.0 and 4.0 half-cell setup). Capacity retention after 100 cycles – 96%, 200 cycles – 90%. The capacity drop at early 30 cycles is due to the side reaction between nanotubes and Li battery electrolyte causing changes in the functional groups of the nanotubes.

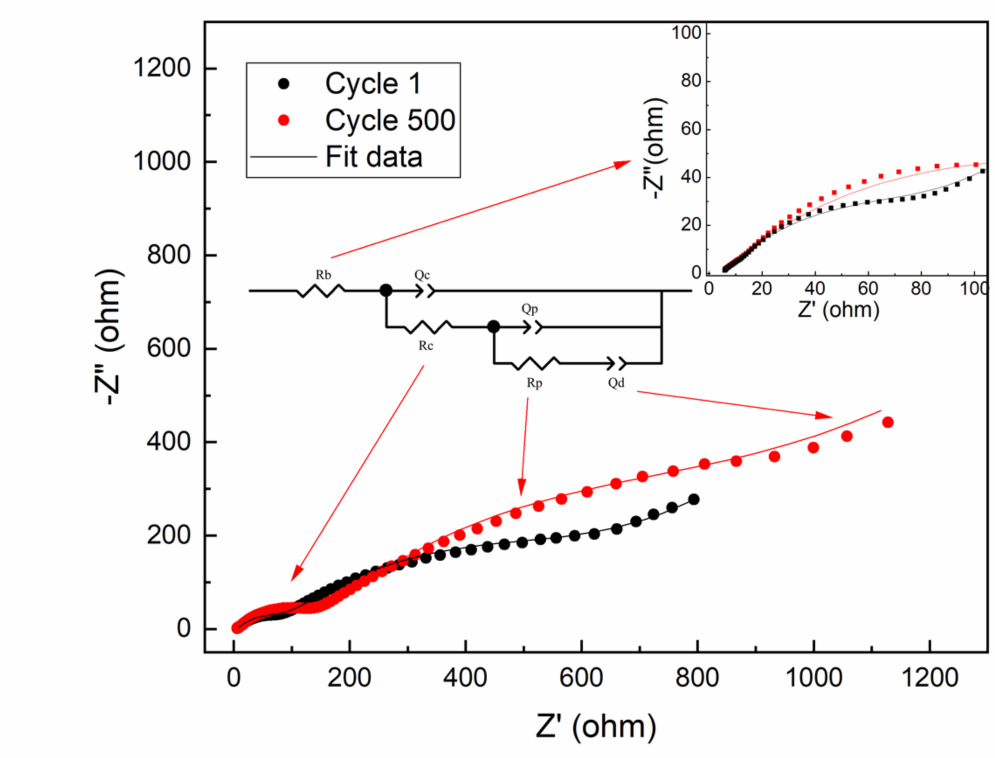

Figure S10. Nyquist plot of the electrochemical impedance spectroscopy (EIS) analysis and corresponding equivalent circuit of the electrochemical processes on V_2O_5/SWCNT before and after the cycling. The EIS spectra have been measured at 2.6 V *vs.* Li^+/Li. R_b –solution resistance, Q_c – current collector – electrode interface capacity, R_c – current collector – electrode interface resistance, Q_p – double layer capacity, R_p – charge transfer resistance, Q_d – diffusion layer capacity.

Table S2. Kinetic parameters of the V_2O_5/SWCNT electrode obtained from fitting the EIS results at 2.6 V *vs.* Li^+/Li. n_c and n_p are roughness parameters (equal to 1 for the ideal capacitor).

	R_b (Ω)	Q_c (F.s$^{(1-nc)}$)	n_c	R_c (Ω)	Q_p (F.s$^{(1-np)}$)	n_p	R_p (Ω)	Q_d (F.s$^{(1-nd)}$)	n_d	Q_p (F.s$^{(1-np)}$)
Cycle 1	6	$9.37\cdot10^{-5}$	0.588	102	$8.42\cdot10^{-4}$	0.579	613	$8.75\cdot10^{-3}$	0.530	6.3
Cycle 500	5	$1.45\cdot10^{-4}$	0.516	197	$9.89\cdot10^{-4}$	0.644	898	$6.01\cdot10^{-3}$	0.497	5.5

The accuracy of each element reported in Table S1 is considered based on the error percentage obtained from the Z-view software. The EIS data were collected at 2.6 V *vs.* Li^+/Li, in which the second lithium (de-)intercalation occurs. One small semicircle and a larger semicircle are detected in the high and medium frequencies, which are followed by a tail at the lowest frequencies. The first semicircle is attributed to the current collector-electrode interface (Q_c, R_c – electrode interface capacity and resistance, respectively) – and the second one is the charge transfer resistance (Q_p – double layer capacity, R_p – charge transfer resistance) of the redox reaction. The sloping behavior at the lowest frequencies could be the diffusion of lithium ions in the electrolyte. Experimental EIS data were analyzed by equivalent circuit modeling (model presented in **Fig. S7** inset) and fitting data for the equivalent circuit elements are presented in **Table S1**. The resistance of the cell is increased after 500 cycles, in which R_c increased from 102 Ω to 197 Ω and the R_p increased from 613 to 898 Ω. These values show that the current collector interface is more affected by cycling than the charge transfer resistance. The reaction between SWCNTs and the electrolyte and formation of the cathode electrolyte interphase layer around the V_2O_5/SWCNT film can cause the increase in the R_c, while degradation and irreversible reduction of the V_2O_5 particles could be the reason for R_p increment.